

Supporting Information

Electronic Properties of Si-H_x Vibrational Modes at Si Waveguide Interface

Muhammad Y. Bashouti,* Peyman Yousefi, Jürgen Ristein and Silke Christiansen

Si Waveguide:

The Si waveguide was fabricated by polish process as shown below (Fig. 1S).

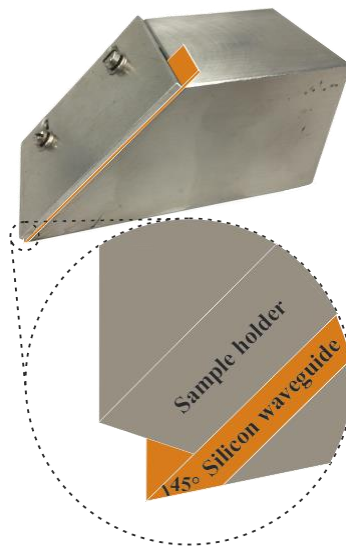


Fig. 1S. Polishing system to fabricate Si waveguide.

A SEM images (top and side view) of the Si waveguide are shown in Fig. 2S. The geometry of the Si waveguide determines the total reflection which in turn determines the sensitivity of the element.

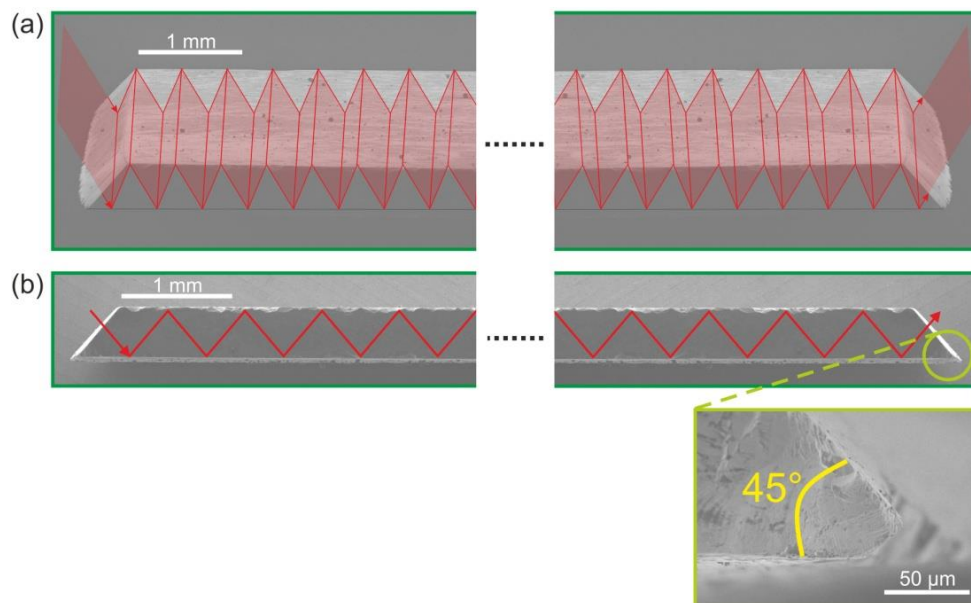


Fig. 2S: SEM of top and side view of the Si waveguide

Critical angle:

The critical angle at which total reflection occurs is dependent on the reflective indices. This can be expressed according to the following equations:

$$\theta_c = \sin^{-1} \left(\frac{n_a}{n_c} \right) \quad \text{eq.1}$$

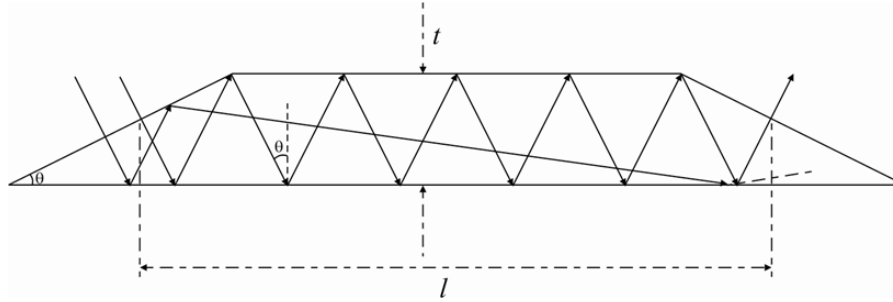


Fig. 3S. Schematic diagram of the total reflection in Si waveguide.

Where θ_c is the critical angle, n_a and n_c are the refractive indices of air and crystal (ATR element), respectively. The refractive index of silicon in mid IR is around 3.4 and the refractive index of air is 1 which means the critical angle is 17° and the total reflection takes place above this angle (cf. Fig. 3S). From engineering consideration, we realized Si waveguide with angle of 45° . The number of total reflection can be calculated according to the geometry of the ATR element:

$$N = \left(\frac{l}{t} \right) \cot \theta_c \quad \text{eq.2}$$

Where N is the number of reflections, l and t are the length and thickness of the ATR element, respectively and θ_c is the critical angle. Since the critical angle is 45° and the thickness and length are 0.525 mm and 49 mm, respectively, we get 93 reflections through our the Si waveguide.

XPS and ATR deconvolution:

Fig. 4S shows the progress of oxidation on H-terminated silicon using the two techniques of XPS and FTIR-ATR. As known, XPS can detect the existence of Si and O atoms on the surface, but not H atoms. On the other hand, ATR in the range of 2000 to 2300 cm^{-1} shows the vibrations of silicon hydrides bonds i.e Si-H_x. Fig. 4S(a) XP spectra of oxide free emission without oxide modes i.e. the initial emission after short HF dip. The deconvolution shows two peaks Si2p_{3/2} at 99.6eV and Si2p_{1/2} at 100.6eV. Fig. 4S(b) shows the relevant ATR of (a) and shows three different modes Si-H, SiH₂ and Si-H₃. Fig. 4S(c) is a representative Si2p emission after 20min annealing in 200 °C. Mix of oxide and oxide free emission are observed:

the Si2p_{3/2} and Si2p_{1/2} emissions and oxide modes as the following: Si₂O at 100.60±0.02 eV; (ii) Si⁺² i.e. SiO at 101.370±0.02, (iii) Si⁺³ i.e. Si₂O₃ at 102.10±0.02eV, and (iv) Si⁺⁴ i.e. (SiO₄) at 103.470±0.02eV. Fig. 5S(d) is the relevant ATR of Fig. 4S(c) and shows the following: Si-H at 2080 cm⁻¹, Si-H₂ at 2110 cm⁻¹, Si-H₃ at 2133 cm⁻¹; oxide modes show two different vibrational modes: SiH₂(O₂) (2200 cm⁻¹) and SiH(O₃) at 2250 cm⁻¹.

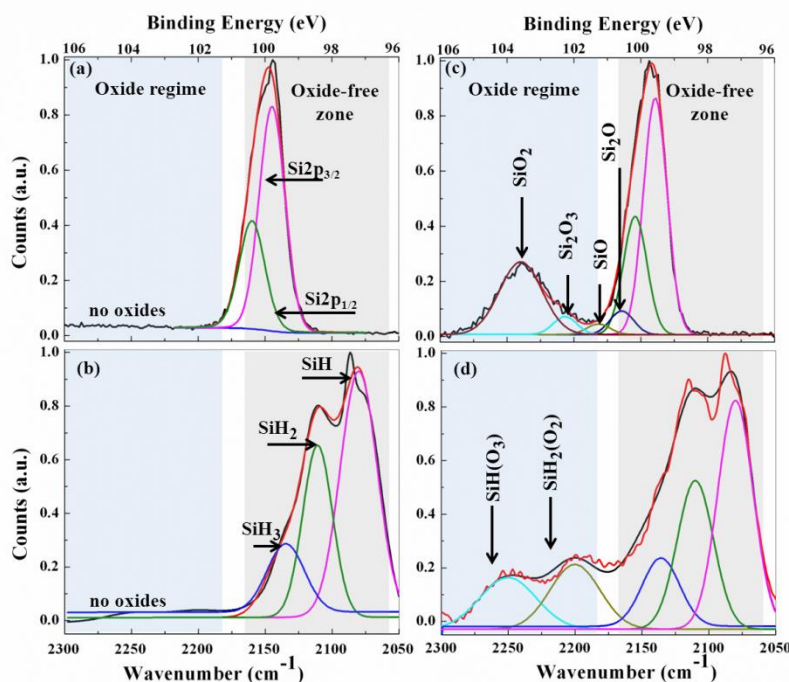


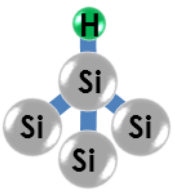
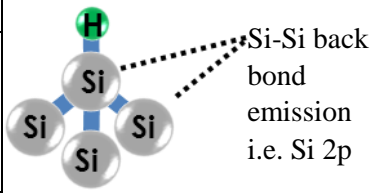
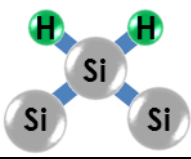
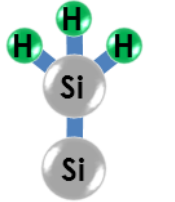
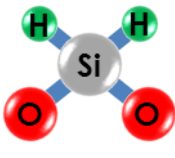
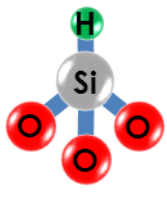
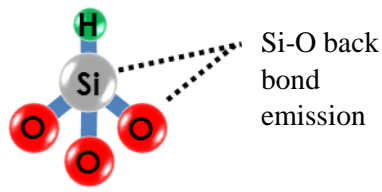
Fig. 4S. Deconvoluted ATR and XP spectra of oxide and oxide free modes on Si waveguide.

For example, for XP spectra, the intensity of the SiH₂(O₂) i.e. (I_{Si+2}) is expressed by the ratio of the integrated area under its peak to the total Si2p emission i.e. oxide free (Si2p_{3/2}+Si2p_{1/2}) and oxide (i.e. Si₂O, SiO, Si₂O₃ and SiO₂) emissions. At the same manner, the observed modes in ATR can be expressed by the ratio of the integrated area to the intensity of all modes i.e. oxide free modes (i.e. SiH₁+SiH₂+SiH₃) and oxide modes, SiH₂(O₂) and SiH(O₃). The intensity of the oxide and oxide free modes as function of time and temperature is shown in Fig. 5S&6S.

Advantage of having in *in situ* measurements:

Inhomogeneity between the samples or dwell time between the measurements or exposing the samples to different environments even for short times will show major differences of each measurement and in this way we cannot correlate the data between the surface characterization tools. Moreover, the inhomogeneity at the sample will make it even hard to follow the changes between the modes and of course quantitative data will not be reliable. To quantitate the work function and fermi level of all the modes, we need to work with same sample at same position. The new technique can be used to analyze more carefully the hybrid surface of semiconductors. Here, we combine three surface analyses tools which shows additional understanding between molecules and interfaces. The new insight of the technique correlates the electronics of the surfaces such as the Iso-point and work function with vibrational modes that would be important to design Schottky barrier and opto-electronic device such as polarized devices.

Table 1S. Structure of the Si-Hx modes (oxide and oxide free modes). The frequencies, binding energy and dipole moment is listed.

Oxide Type	Mode	Structure and moment dipole	Binding Energy
Oxide Free Modes	Si-H (2080cm ⁻¹)	 D= 0.11 D	The emission of the Si-Si back bonds at Si2p _{3/2} (99.60±0.02eV) and Si2p _{1/2} (99.30±0.02eV). Example for Si-Si emission:  Si-Si back bond emission i.e. Si 2p
	SiH ₂ (2110 cm ⁻¹)	 D= 0.06 D	
	SiH ₃ (2133cm ⁻¹)	 D=0.0D	
Oxide Modes	-	Very low intensity	Si ₂ O i.e. Si ⁺¹ at 101.2 ±0.02eV
	SiH ₂ (O ₂) (2200cm ⁻¹)	 D=1.59 D	SiO i.e. Si ⁺² at 101.7±0.02eV
	SiH(O ₃) (2250cm ⁻¹)	 D=2.13D	Si ₂ O ₃ i.e. Si ⁺³ at 102.7±0.02eV Example of Si-O bond emission:  Si-O back bond emission
	-	No mode (no hydrogen left)	SiO ₂ i.e. Si ⁺⁴ at 103.6±0.4eV

Si-O modes Vs Si-H modes:

Si-O modes (at $1050\text{--}1080\text{ cm}^{-1}$) can be used to follow the kinetics of hydrogen and oxygen diffusion and to correlate them with Si-H modes. However, Si-O modes do not include all the hydrogen modes and would be very hard to follow the modes or the transfer between modes or the kinetics of hydrogen detaching.

Oxide-Free Modes:

Fig. 5S shows the normalized intensity of oxide free modes (Si-H and Si-H₂) as function of the temperature and time. As show, the intensity of Si-H and Si-H₂ decreases quickly in high temperatures and slowly in low temperature. For example, at 100 °C, the Intensity of Si-H and SiH₂ decreased 15% and 5% after 10 min, while at 500 °C decreased by 95% for both. Interestingly the Si-H₂ are more stable than Si-H. As known, Si (100) prefers forming Si-H₂. i.e. silicon forms dimer bonds leading to the formation of SiH₂. (J. Appl. Phys. 79 (8), 15 April 1996).

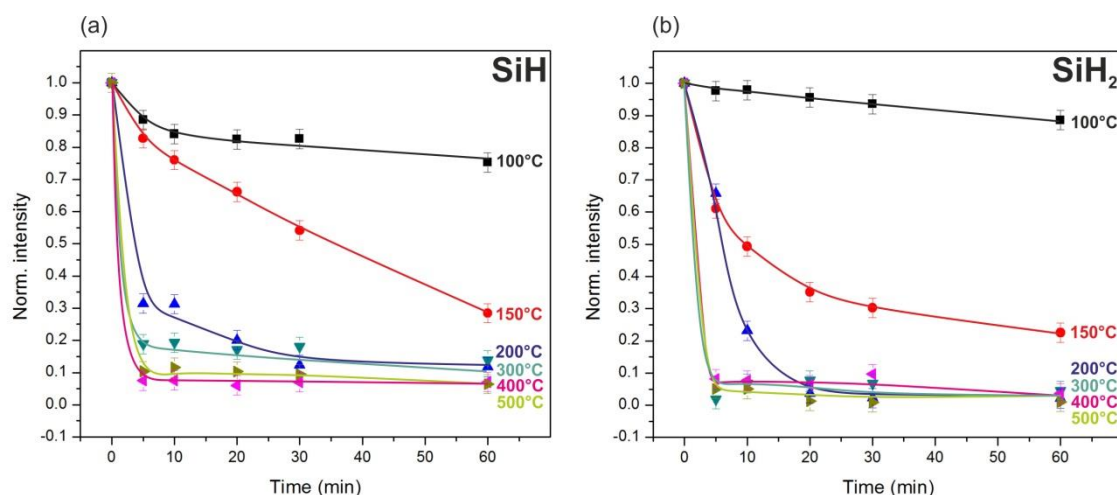


Fig. 5S. Normalized intensity of Si-H and SiH₂ at different temperatures and time. (a) for Si-H, and (b) for Si-H₂.

Oxide-Modes:

Fig. 6S shows the normalized intensity of oxide modes (SiH₂(O₂) and Si-H(O₃)) as function of the temperature and time. Both plots have been normalized to their maximum values after 5min to show their evaluation as function of temperature and time. Both show an immediate increase 0-5min, then a decay. It should be noted that the maximum intensity SiH(O₃) at high temperature is ~5 times higher than SiH₂(O₂). This implies that SiH(O₃) more stable than SiH₂(O₂) which decompose to form the SiH(O₃) as proposed as transformation mechanism from SiH₂(O₂) to SiH(O₃).

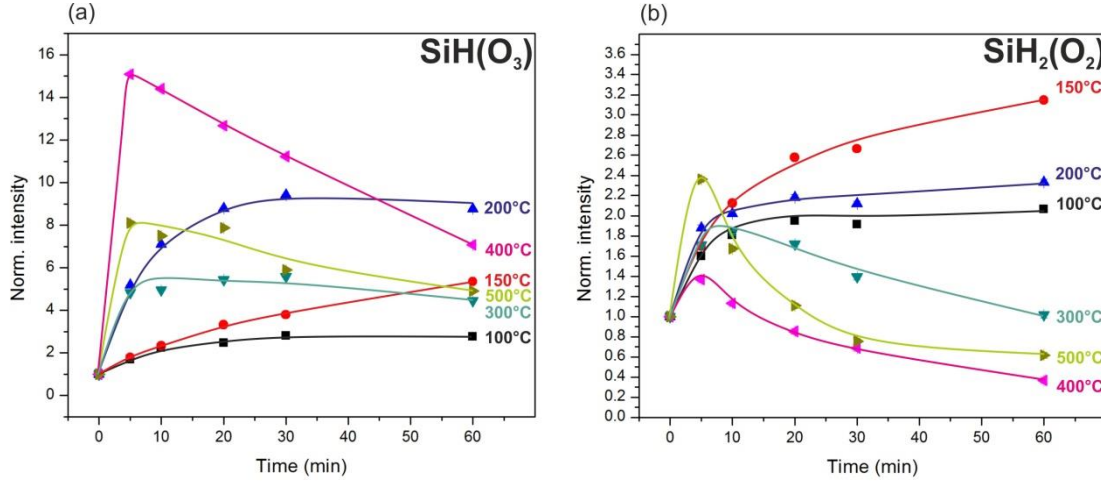


Fig. 6S. Normalized intensity of oxide modes at different temperatures and time of annealing: (a) for SiH(O₃), and (b) for SiH₂(O₂).

Total oxidation (%)

Total oxidation (%) can be calculated by H-removal (%) and O-diffusion (%). The H-removal (%) is as follows:

$$\text{H-removal (\%)} = -(I_{(\text{Free mode})t>0} - I_{(\text{Free mode})t=0})$$

Here, $I_{(\text{Free mode})t=0}$ is the normalized intensity of the oxide free modes immediately after HF i.e. the modes did not exposure or anneal, thus $I_{(\text{Free mode})t=0} = 100\%$. After the modes exposed $t>0\text{min}$, or annealed $T \geq 100^\circ\text{C}$, the normalized intensity of the oxide free modes decreases and termed as $I_{(\text{Free mode})t>0}$.

$$\text{O-diffusion (\%)} = I_{(\text{oxide mode})t>0} - I_{(\text{oxide mode})t=0}$$

Here, $I_{(\text{oxide mode})t=0}$ is the normalized intensity of the oxide free modes immediately after HF i.e. the modes did not exposure or anneal, thus $I_{(\text{Free mode})t=0} = 0\%$. After the modes exposed $t>0\text{min}$, or annealed $T \geq 100^\circ\text{C}$, the normalized intensity of the oxide modes increases and termed as $I_{(\text{oxide mode})t>0}$. (cf. Fig. 7S). Briefly, the H-removal and O-diffusion percentages are equal to the related modes intensity difference between the modes intensity after annealing (or exposure time) with their intensity after immediate HF.

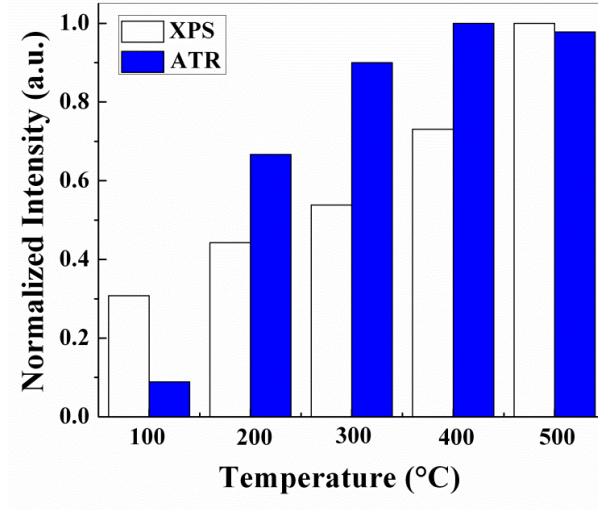


Fig. 7S. Normalized oxide intensity as obtained in ATR and XP spectra.

The oxidation mechanism is schematically drawn in Fig. 8S. As shown, firstly oxide free modes were realized after HF dip. Secondly, these modes can be oxidized by two different mechanisms. (H-removal and O-diffusion).

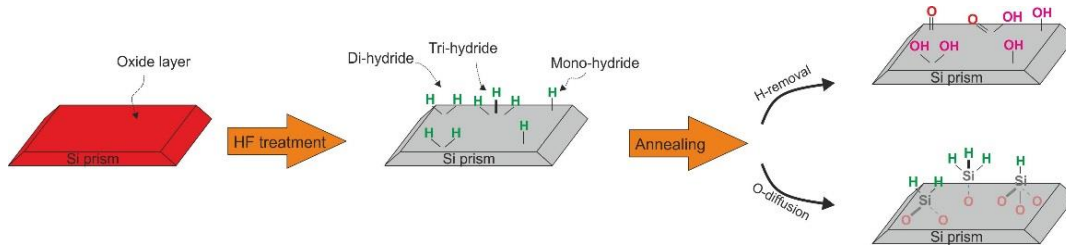


Fig. 8S. Si waveguide with native oxide was etched by etchant solution of HF:NH₄F, 1:6 to remove all the oxide layers and contaminations to realize oxide free modes. The post annealing shown two possible oxidation mechanisms: H-removal and O-diffusion.

Induction model

The oxide modes show higher vibrational wavenumber than oxide free mode. The frequency of each mode is dependent on the number of oxygen atoms bonded to the central silicon atoms. Smith et. al. and Lucovsky et. al. proposed (induction model) that correlate the frequency of the Si-H_x modes with the number of diffused oxygen atoms to the back-bonds. The total electronegativity of atoms surrounding a Si atom is defining the Si-H bond length.^[1] The higher the total electronegativity the shorter the Si-H bond length, as a result, the modes vibrates at higher frequencies. Lucovsky proposed the following empirical equation and applied his model to wide variety of Si-H_x modes and silane molecules:

$$\nu_{Si-H} = a + b \sum_{j=1}^3 SR(R_j) \quad \text{Eq. 3}$$

Where a and b are constants, and $SR(R_j)$ is the stability ratio which is based on Pauling's electronegativity, $X(A_j)$. The empirical relation between those two is given by:

$$[X(A_j)]^{1/2} = 0.21SR(R_j) + 0.77 \quad \text{Eq. 4}$$

$SR(R_j)$ is stability ratio of the respected molecule (or mode) which can be calculated according to the following equation:

$$SR(R_j) = \frac{[X(A_j)]^{1/2} - 0.77}{0.21}$$

Where, $X(A_j)$ is Pauling's electronegativity of the respected atom. The following expressions describe the vibration frequencies for mono- and di-hydrides.

$$\begin{aligned} \nu_{Si-H}(SiH) &= 1740.7 + 34.7 \sum_{j=1}^3 SR(R_j) \\ \nu_{Si-H}(SiH_2) &= 1956.3 + 25.4 \sum_{j=1}^2 SR(R_j) \end{aligned}$$

The induction model takes into account the nearest neighbor interaction and the next nearest atoms. It has been demonstrated that Si-H vibrational frequencies are dependent on the chemical bond with their next nearest environment and the Si-H bonding distance decreases from 1.50 to 1.46 Å as the number of oxygen atoms in the next nearest neighbors' increases from 0 to 3. According to the induction model, insertion of more electronegative atoms into the main substrate reduces the distance between atoms and makes the molecular bonds stronger. As a result, those bonds need higher energy to vibrate (i.e. wavenumbers). In our case, SiH_3 oxidized to be $SiHO_3$ and SiH_2 oxidized to be $SiH_2(O_2)$, while their frequencies shifted from 2110 cm^{-1} to 2200 cm^{-1} and from 2133 cm^{-1} to 2275 cm^{-1} , respectively.

Vibration Wavenumber Shift:

Comparing the two oxide modes i.e. $SiH(O_3)$ and $SiH_2(O_2)$ with SiH_x , one can observe a shift in the vibration frequencies from $\sim 2100 \text{ cm}^{-1}$ to $\sim 2250 \text{ cm}^{-1}$ (Fig. 9S).

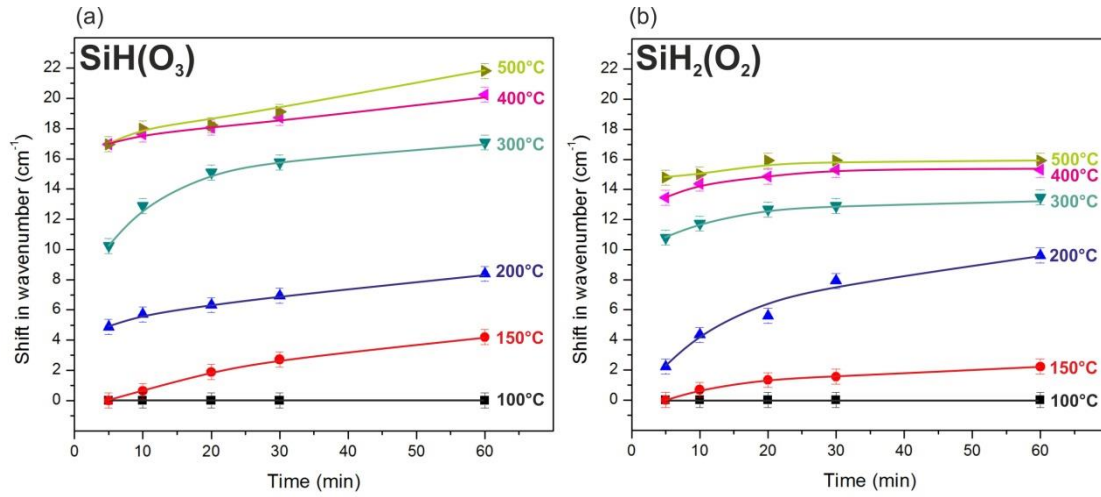


Fig. 9S. Vibration wavenumber at different temperatures and time, for (a) Si-H(O₃), and (b) Si-H₂(O₂).

The large shift explained by induction insertion oxygen atoms to the back-bonds as know “Induction Model”. The shift dependent mainly on the temperature (varying the time from 0-60min shifts the mode by $\pm 2\text{cm}^{-1}$). The highest shift is shown in the saturated oxide mode i.e, SiH(O₃) which shifted by 22 cm^{-1} while SiH₂(O₂) by 16 cm^{-1} .

Table 2S: Electronic properties (work function, affinity and surface dipoles) of the oxide and oxide free modes at different temperatures 100-500°C.

data from ATR		Electronic Properties (in eV units)			
T	ATR	Si2p _{3/2}	Φ	χ	Surface dipoles
100	0	99.78	4.04	3.98	-0.07
200	0.03	99.69	4.21	4.06	0.01
300	0.21	99.65	4.39	4.2	0.15
400	0.665	99.6	4.5	4.26	0.21
500	1	99.52	4.57	4.25	0.2

Iso-Point: At the iso point, the net dipole is zero, however, the work function is not similar to the bare silicon. Our measured work function was 4.21eV which differ by 0.16eV from the bare Si which may due to band bending induced by the dipoles.

Growth Rate:

Fig. 10S shows the growth of the oxides modes from their relative oxide free modes. As shown, the SiH₂ decay's rapidly to form SiH₂(O₂), while SiH(O₃) is slowly formed. The growth rate at different conditions is illustrated in Fig. 11S. At lower oxide intensity (0-0.4), the growth rate of SiH(O₃) and SiH₂(O₂) are almost equal (± 0.02). However, as the oxide intensity increased, (0.6-1), the growth rate of SiH₂(O₂) decreases dramatically (± 0.1) while SiH(O₃) remain with minor decay (± 0.02). On the other hand, the growth rate of SiH(O₃)

increases for 10, 20 and 30 min of annealing after reaching to the 0.6 oxide intensity point. This value for 5 min and 60 min has a slight decrease though.

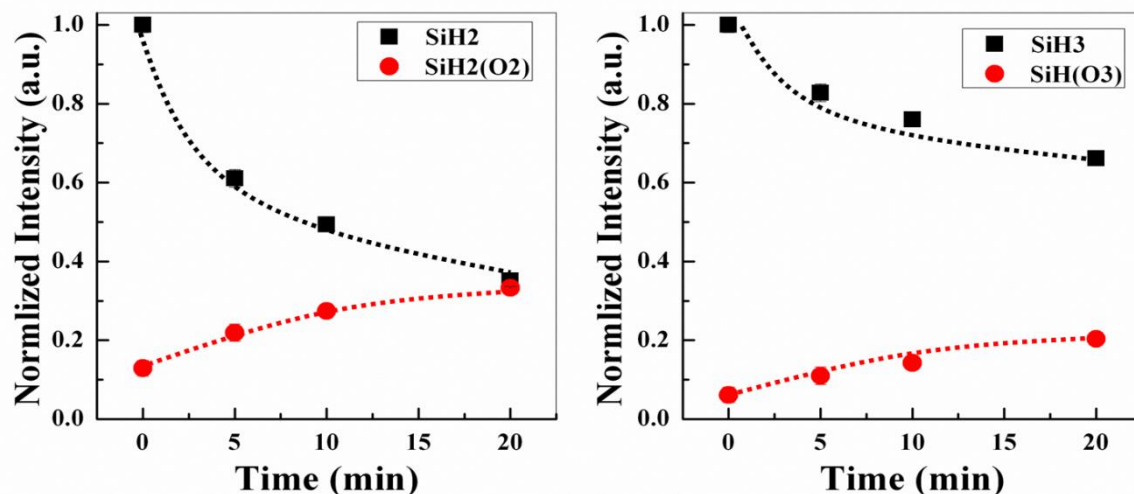


Fig. 10S. Kinetics of oxide and oxide free modes at contact temp (200) as function of time 0-20min.

This behavior implies the existence of two distinct mechanisms: Oxygen diffusion through SiH and SiH₂O₂ at lower oxide intensities and a transformation mechanism from SiH₂(O₂) to SiH(O₃) at critical times and oxide intensities (10 to 30 min by more than 0.6 oxide intensity).

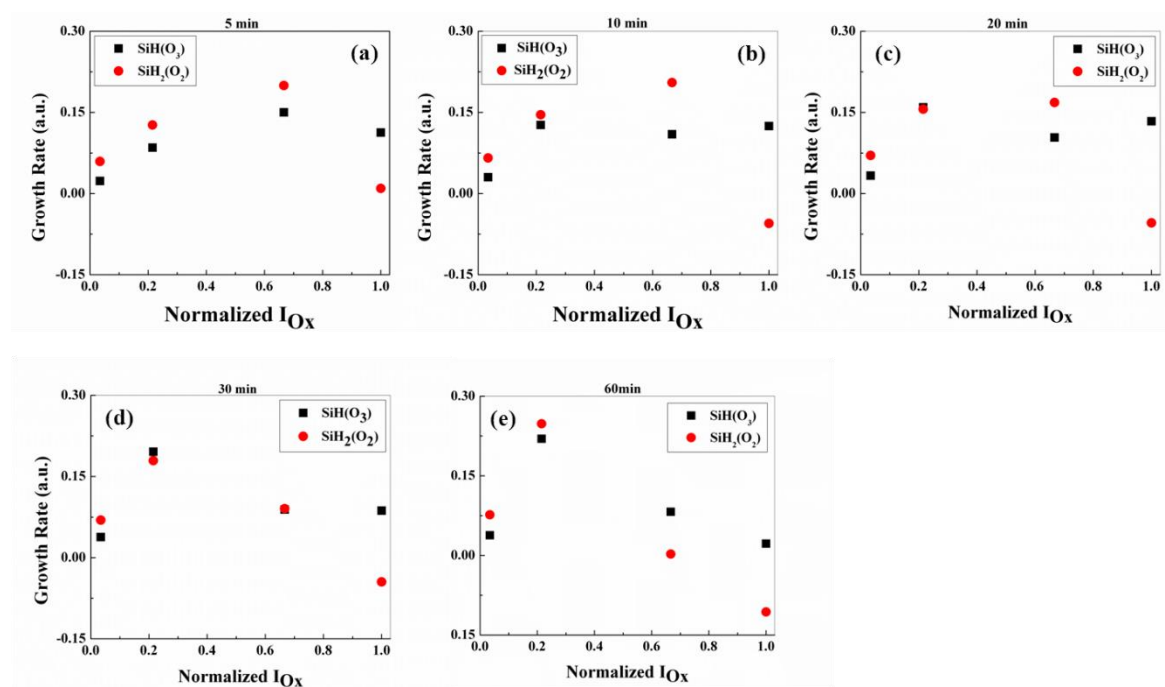


Fig. 11S. Growth rate of SiH(O₃) and SiH₂(O₂) at different times and temperatures. Temperatures are presented as the oxide intensities.

Experimental section:

Internal reflection element (IRE): was made from a single side polished n-doped Si(100) ($\rho=1-5 \text{ } \Omega\text{cm}$) wafer. After polishing the other side by diamond emulsion, two edges of the rectangular shaped silicon wafer were bevelled to 45° by using a special holder shown in fig. S1. Dimensions of the IRE were $49 \times 19 \times 0.525 \text{ mm}^3$. The final shape of our IRE is illustrated in fig. 1. The IRE surface was cleaned by acetone and isopropanol respectively in ultrasonic bath. An etchant buffer solution of HF:NH₄F (1:6) was used to remove the native oxide. The sample was dipped into the etchant for 30 sec, cleaned by H₂O and dried by N₂. Temperatures of 100°C, 150°C, 200°C, 300°C, 400°C and 500°C with the time spans of 5 min, 10 min, 20 min, 30 min and 60 min were chosen as the annealing conditions.

Internal reflection element (IRE): was made from a single side polished n-doped Si(100) ($\rho=1-5 \text{ } \Omega\text{cm}$) wafer. After polishing the other side by diamond emulsion, two edges of the rectangular shaped silicon wafer were bevelled to 45° by using a special holder shown in fig. S1. Dimensions of the IRE were $49 \times 19 \times 0.525 \text{ mm}^3$. The final shape of our IRE is illustrated in fig. 1. The IRE surface was cleaned by acetone and isopropanol respectively in ultrasonic bath. An etchant buffer solution of HF:NH₄F (1:6) was used to remove the native oxide. The sample was dipped into the etchant for 30 sec, cleaned by H₂O and dried by N₂. Temperatures of 100°C, 150°C, 200°C, 300°C, 400°C and 500°C with the time spans of 5 min, 10 min, 20 min, 30 min and 60 min were chosen as the annealing conditions.

X-ray photoelectron spectroscopy: Core level and valance band photoelectron spectra were excited by monochromatic Al K radiation (1487 eV) and minimize the effect of X-ray damage due to the sample collected with an adjustable overall resolution between 0.8 and 1.2 eV. Photoelectrons were picked up at a takeoff angle of 35° enhancing the surface sensitivity of the technique to about 10-15 Å depth. Samples were first scanned from 0 to 1000 eV to monitor signals for C, O and Si. The Si2p at 98.0-105.0 eV, C1s at 282.0-287.0 eV, O1s at 520-550 eV and valance band emission (0-35eV, 200 scans) were investigated in detail. Scan times of up to ~2 h were employed for all data collections except of and emission data that takes integration times of ~8 h. Data analysis was performed using the Sigma Probe Advantage software. Precise binding energy positions and intensities were calculated by peak fitting using software package (XPSPEAK version 4.1). Peak fitting solutions

were sought for $\chi^2 < 1$, where χ^2 stands for the standard deviation. For the Si 2p band at 99.5eV we actually deconvolute two spin orbit-doublets with an energy splitting of 0.6 eV. This energy splitting originates from binding energy differences of bulk Si atoms and surface Si atoms. The observed binding energy of the Si 2p_{3/2} bulk signal allows determining the difference between the Fermi level and the energy of the valance-band maximum at the surface. The integral areas under specific peaks of the XPS spectra were normalized to the integral under the Si 2p peak (sum of Si 2p_{1/2} and Si 2p_{3/2} *i.e.* the none oxidized silicon atoms) and adjusted with respect to scan time.

Work Function Measurements by the Kelvin Probe Method: The work functions of the samples were determined by measuring the contact potential difference (CPD) with respect to a 3mm circular and semi-transparent probe by the Kelvin probe method. The work function of this probe was measured and regularly confirmed in calibration experiments with an evaporated Au film whose work function was determined by its photoelectron yield spectra fitted to a Fowler type shape that is valid for metals in a very good approximation. The overall accuracy of this technique can be estimated to about ± 30 meV for the work function data obtained.

ATR-FTIR spectroscopy: ATR-FTIR spectroscopy in the range of mid-Infrared was applied to explore the vibrations from 400 to 4000 cm⁻¹. Sample environment was getting purged by dry air for 5 min before each measurement. A liquid air cooled HgCdTe detector was used. Resolution of 2 cm⁻¹ and 100 times of scans were performed for each measurement. The filler apodization was used to have less-signal to noise ratio.

References:

[1] N. J. Harrick, Internal Reflection Spectroscopy, New York: John Wiley & Sons, 1987.